

ARTICLE

Received 23 Sep 2013 | Accepted 24 Mar 2014 | Published 25 Apr 2014

DOI: 10.1038/ncomms4711

Dynamic competition between spin-density wave order and superconductivity in underdoped $\text{Ba}_{1-x}\text{K}_x\text{Fe}_2\text{As}_2$

M. Yi^{1,2}, Y. Zhang^{1,3}, Z.-K. Liu^{1,2}, X. Ding⁴, J.-H. Chu⁵, A.F. Kemper⁶, N. Plonka^{1,2}, B. Moritz^{1,7}, M. Hashimoto⁸, S.-K. Mo³, Z. Hussain³, T.P. Devereaux¹, I.R. Fisher^{1,2}, H.H. Wen⁴, Z.-X. Shen^{1,2} & D.H. Lu⁸

An intriguing aspect of unconventional superconductivity is that it always appears in the vicinity of other competing phases, whose suppression brings the full emergence of superconductivity. In the iron pnictides, these competing phases are marked by a tetragonal-to-orthorhombic structural transition and a collinear spin-density wave (SDW) transition. There has been macroscopic evidence for competition between these phases and superconductivity as the magnitude of both the orthorhombicity and magnetic moment are suppressed in the superconducting state. Here, using angle-resolved photoemission spectroscopy on detwinned underdoped $\text{Ba}_{1-x}\text{K}_x\text{Fe}_2\text{As}_2$, we observe a coexistence of both the SDW gap and superconducting gap in the same electronic structure. Furthermore, our data reveal that following the onset of superconductivity, the SDW gap decreases in magnitude and shifts in a direction consistent with a reduction of the orbital anisotropy. This observation provides direct spectroscopic evidence for the dynamic competition between superconductivity and both SDW and electronic nematic orders in these materials.

¹Stanford Institute for Materials and Energy Sciences, SLAC National Accelerator Laboratory and Stanford University, Menlo Park, California 94025, USA.

²Departments of Physics and Applied Physics, and Geballe Laboratory for Advanced Materials, Stanford University, Stanford, California 94305, USA.

³Advanced Light Source, Lawrence Berkeley National Laboratory, Berkeley, California 94720, USA. ⁴Center for Superconducting Physics and Materials, National Laboratory of Solid State Microstructures and Department of Physics, National Center of Microstructures and Quantum Manipulation, Nanjing University, Nanjing 210093, China. ⁵Department of Physics, University of California, Berkeley, California 94720, USA. ⁶Computational Research Division, Lawrence Berkeley National Laboratory, Berkeley, California 94720, USA. ⁷Department of Physics and Astrophysics, University of North Dakota, Grand Forks, North Dakota 58202, USA. ⁸Stanford Synchrotron Radiation Lightsource, SLAC National Accelerator Laboratory, Menlo Park, California 94025, USA. Correspondence and requests for materials should be addressed to D.H.L. (email: dhlu@slac.stanford.edu) or to Z.-X.S. (email: zxshen@stanford.edu).

To understand the phenomenon of high-temperature superconductivity (HTSC), it is important to understand the competing states of the superconducting phase. In both families of HTSC materials, the competing states consist of various symmetry-breaking phases, which interact with superconductivity (SC) in intricate ways. In the cuprates, one of the biggest puzzles is the nature of the pseudogap (PG) phase, which envelops a large portion of the superconducting dome in the phase diagram. Recently, a large amount of experimental evidence suggests a competition between the PG and SC^{1–4}. However, the controversial nature of the PG phase itself complicates a direct study of this competition. Conversely, in the iron pnictides, the competing phases are well characterized: a collinear spin-density wave (SDW) order has been well established as the main competing phase in the underdoped (UD) region of iron pnictides^{5,6}, while a nematic phase associated with the structure transition (T_S) has been suggested as another competing phase^{7–11}. The two transitions associated with these competing orders track each other closely, occurring either simultaneously or with T_S preceding T_{SDW} . SC emerges as these phases are suppressed with carrier doping, isovalent substitution, or pressure^{12,13}. The way in which these two orders interact with SC varies among the pnictide families: while SC and SDW exhibit mutual exclusion in the $LnFeAsO$ families¹⁴, there is a large region of coexistence in both the $NaFeAs$ ¹⁵ and the $BaFe_2As_2$ families^{16–18}. In addition, transport and neutron scattering experiments have shown that the orthorhombicity and magnetic moment, which are the macroscopic order parameters for the structural and SDW orders, are suppressed with the onset of SC^{19–21}, signalling macroscopic competition between these orders and SC.

In this paper, we focus on the phase competition between these orders and SC, which makes UD $Ba_{1-x}K_xFe_2As_2$ in the coexistence region an ideal candidate as T_S/T_{SDW} and T_C are well separated; yet, T_C is sufficiently high to be experimentally accessible¹⁸. In particular, we study the electronic structure of a UD compound ($x=0.15$), where $T_S = T_{SDW} = 110$ K and $T_C = 14.5$ K, and the non-superconducting undoped $BaFe_2As_2$ compound ($x=0$) with $T_S = T_{SDW} = 138$ K for comparison. Using high-resolution angle-resolved photoemission spectroscopy (ARPES), we directly observe the electronic response of each order in this compound. Distinct spectral signatures of the three orders are observed to coexist on the same electronic structure below T_C , signalling the microscopic coexistence of the three orders. More importantly, we observe the spectral gap associated with the SDW order to be suppressed with the onset of SC. Furthermore, using a tight-binding model, we show that a reduction in the nematic order parameter is also needed to fully account for the observed shift of the SDW gap below T_C . These observations show a direct electronic competition between the SDW and nematic orders with SC in $Ba_{1-x}K_xFe_2As_2$.

Results

Spectral evolution across phase transitions. The momentum-resolved electronic structure, which can be directly imaged by ARPES, is expected to undergo distinct changes at each of the transitions in the system. As illustrated in the generic schematic in Fig. 1b, starting in the normal state ($T > T_S, T_{SDW}$), the typical electronic structure of iron pnictides consists of hole bands at the Brillouin zone (BZ) centre, Γ point, and electron bands at the BZ corner, X point. Lowering the temperature approaching T_S , orbital-dependent band shifts onset, as has been observed in Co-doped $BaFe_2As_2$ (ref. 9) and $NaFeAs$ ²², where bands dominated by the d_{xz} (d_{yz}) orbital character shift down (up) in a k -dependent fashion (minimal at Γ and maximal at X , see Supplementary

Fig. 1; Supplementary Note 1), breaking C_4 rotational symmetry. Across T_{SDW} , translational symmetry is broken and bands fold along $Q_{SDW} = (\pi, \pi)$, opening SDW gaps such that the Fermi surface reconstructs, leaving portions ungapped. Finally, as the system is cooled below T_C , particle-hole symmetric superconducting gaps open on bands that cross the Fermi level, E_F . Hence, there are distinct spectroscopic signatures associated with the three order parameters in this system.

To avoid twinning effects in the orthorhombic state, all measurements were performed on mechanically detwinned samples held under uniaxial stress. Although the effect of the detwinning stress on the transition temperatures has not been systematically studied in the $Ba_{1-x}K_xFe_2As_2$ system, such a study in the $Ba(Fe_{1-x}Co_x)_2As_2$ system shows that the stress naturally broadens T_S to higher temperature⁷, but does not affect the full magnitude of the orbital anisotropy at the lowest temperature⁹; (Supplementary Note 1). Furthermore, in a systematic study in the $BaFe_2(As_{1-x}P_x)_2$ system, it is shown that the mechanical detwinning stress increases T_{SDW} and decreases T_C (ref. 23). In the current study, we do not observe any significant modification of T_{SDW} and T_C within experimental uncertainties inferred from the temperatures at which spectral features associated with these orders onset compared with those measured on unstressed crystals.

Figure 1c shows the changes observed across T_S/T_{SDW} for the UD sample. In the normal state, the $\Gamma - X$ and $\Gamma - Y$ directions are degenerate, respecting C_4 symmetry. Lowering temperature below T_S/T_{SDW} lifts this degeneracy, leading to the observed C_4 symmetry breaking. More specifically, measuring band dispersion with light polarized perpendicular to the cut direction (Fig. 1d upper panels) reveals that the hole-like band with predominantly d_{yz} character along the antiferromagnetic (AFM) direction near X moves to higher energy than the corresponding d_{xz} band along the ferromagnetic (FM) direction near Y , a signature of the orbital anisotropy seen in the nematic phase of Co-doped $BaFe_2As_2$ (ref. 9). In fact, the magnitudes of the orbital energy splitting in the K-doped samples are comparable to those in Co-doped samples, and roughly scale with T_S independent of the type of doping (Supplementary Fig. 2). Furthermore, electron bands folded from the BZ corner can be observed at the Γ point, indicative of long-range SDW order. These signatures of the nematic and SDW orders in the UD case are very similar to those observed in $BaFe_2As_2$, as a chemical potential shift of ~ 50 meV roughly mimics the doping effect between $BaFe_2As_2$ and the UD sample (Supplementary Note 1).

SDW gaps open where the folded electron bands cross the hole bands near Γ (Fig. 2). In $BaFe_2As_2$, the SDW gaps can be seen around -60 meV and -15 meV along those cuts (Fig. 2a). Focusing on the deeper SDW gap, the gap opens at T_{SDW} and monotonically increases with lowering temperature as no other transitions exist below T_{SDW} , similarly to the behaviour of the magnetic moment^{20,21}. The more interesting case occurs in the UD compound, in which an SDW gap around -15 meV corresponds to the one discussed in $BaFe_2As_2$. Figure 2c,d compare the evolution of this SDW gap above (20 K) and below (5 K) T_C , where the bands forming the gap are marked. Cooling the sample below T_C , the SDW gap magnitude abruptly decreases, which can be better visualized in two ways. First, comparing the energy distribution curves (EDC) above and below T_C (Fig. 2e), we see two changes: (i) at k_F where the upper band crosses E_F , a SC gap opens (circles); (ii) the lower band shifts up in energy (dashed curves), reducing the effective SDW gap size. Secondly, we can examine the momentum distribution curves, which are horizontal line cuts through the spectra images in Fig. 2c,d. We fit these momentum distribution curves with Lorentzians for the two hole bands (Supplementary Note 2). As the bands are relatively

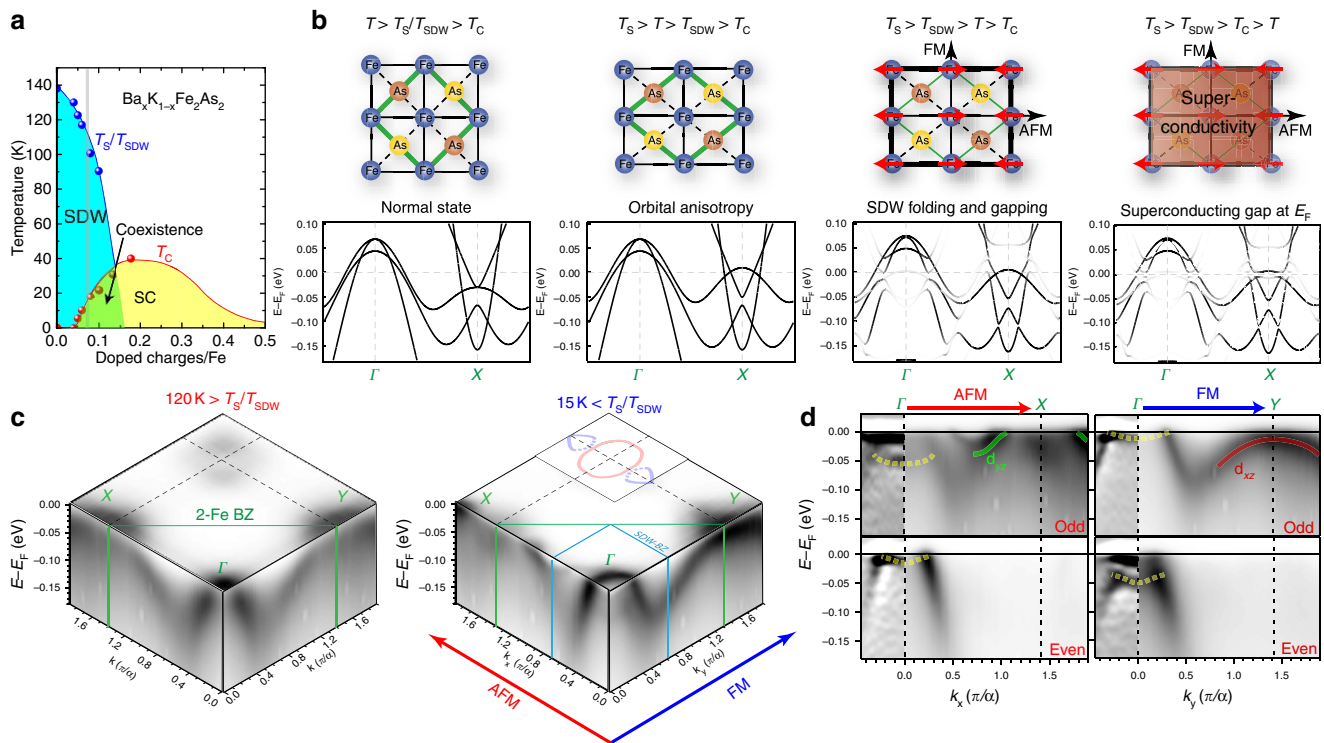


Figure 1 | Schematic and spectral evolution across phase transitions. (a) Phase diagram of $Ba_{1-x}K_xFe_2As_2$ adapted from ref. 18, where the grey vertical line indicates the doping of the UD compound studied. (b) Schematic of the expected evolution of the band structure across T_S , T_{SDW} and T_C . From left to right, the four panels exhibit the band structure along the high-symmetry direction Γ -X in the 2-Fe BZ, starting with the normal state ($T > T_S, T_{SDW}$), with the incremental addition of orbital anisotropy ($T_S > T > T_{SDW}$), SDW folding and gapping ($T_S/T_{SDW} > T > T_C$) and finally SC ($T < T_C$). (c) Measured electronic structure (Fermi surface and band dispersions) in the normal state and SDW state (below T_S/T_{SDW} but above T_C) of the UD compound, with mixed even and odd light polarization. The reconstructed Fermi surface in the SDW state is outlined. (d) Band dispersions measured with purely even or odd polarization along the AFM and FM directions in the SDW state at 15 K. The $k < 0$ portions are second energy derivatives of the raw spectra. The hole-like band identified as d_{yz} along AFM and d_{xz} along FM are labelled, signalling the electronic nematicity. The electron bands folded from the X point to the Γ point are marked with yellow dotted curves. All measurements were taken with 47.5 eV photons.

steep, the fitted positions would trace out the underlying ungapped band dispersion, while the fitted intensity of the inner hole band would show a suppression within the energy range in which the SDW gap develops. The fitted intensity for the inner hole band is plotted in Fig. 2g for the two temperatures, where the separation between the two peaks is another measurement of the SDW gap, which clearly decreases below T_C .

Model simulation. To better understand this decrease in the SDW gap below T_C , we have simulated the spectroscopic effects of three order parameters (Δ_S , Δ_{SDW} , Δ_{SC}) associated with the three transitions (T_S , T_{SDW} , T_C) based on a five-orbital tight-binding model of $BaFe_2As_2$ from density-functional theory (DFT) band structure²⁴, which is shifted by 0.15 eV and renormalized by a factor of 3 to match the observed band structure for the UD compound. The order parameters are incorporated phenomenologically, with Δ_S introduced as an orbital-dependent on-site energy shift between d_{xz}/d_{yz} that is momentum dependent (zero at Γ and maximal at X/Y); Δ_{SDW} as an interaction term in the orbital basis; and Δ_{SC} as a particle-hole symmetric isotropic gap at E_F . We examine the calculated band dispersions near Γ along the same cut as the data in Fig. 2c. Figure 3a displays the situation deep in the orthorhombic SDW state but still above T_C , with finite values for Δ_S and Δ_{SDW} . Here, we highlight in pink the SDW gap formed between the inner hole band and the folded electron band similar to the one observed experimentally in Fig. 2c. In the simplest scenario with no

competition and SC added directly (Fig. 3b), only bands near E_F are affected by the opening of a SC gap, with little effect on the observed SDW gap. In particular, the lower branch does not shift up, contrary to experimental observation. To account for the observed reduction in the SDW gap below T_C , Δ_{SDW} needs to be reduced before adding Δ_{SC} (Fig. 3c). However, the centre of the gap does not shift noticeably relative to that above T_C , whereas in the data, an overall shift towards E_F is also observed in addition to the reduced gap size. To reproduce this shift, an additional reduction in Δ_S is required (Fig. 3d). The best match to the experimental data is obtained by introducing a moderate reduction in both Δ_{SDW} and Δ_S (Fig. 3e). In reality, these two order parameters are intimately connected, as one enhances the other²⁵⁻²⁷. It is intrinsically difficult to separate these two effects, but the exercise displayed in Fig. 3 demonstrates the qualitative effects on the electronic structure of reducing each order parameter, and gives an intuitive understanding of the combined suppression of both orders below T_C . Here, we note that the observed SDW gap shrinks in magnitude, as seen in the shift of the EDC peaks marking the boundary of the gap. This is the behaviour expected of the spectral evolution of a generic order parameter in competition. We note that our theoretical model here is based on an itinerant origin of the magnetism, while the general nature of magnetism in iron pnictides has not been fully settled, with proposals for coexistence of both itinerant and local magnetism²⁸. In this regard, our observation of the reduction of the SDW gap itself shows a general competition of SC and SDW independent of the nature of the magnetism, as the

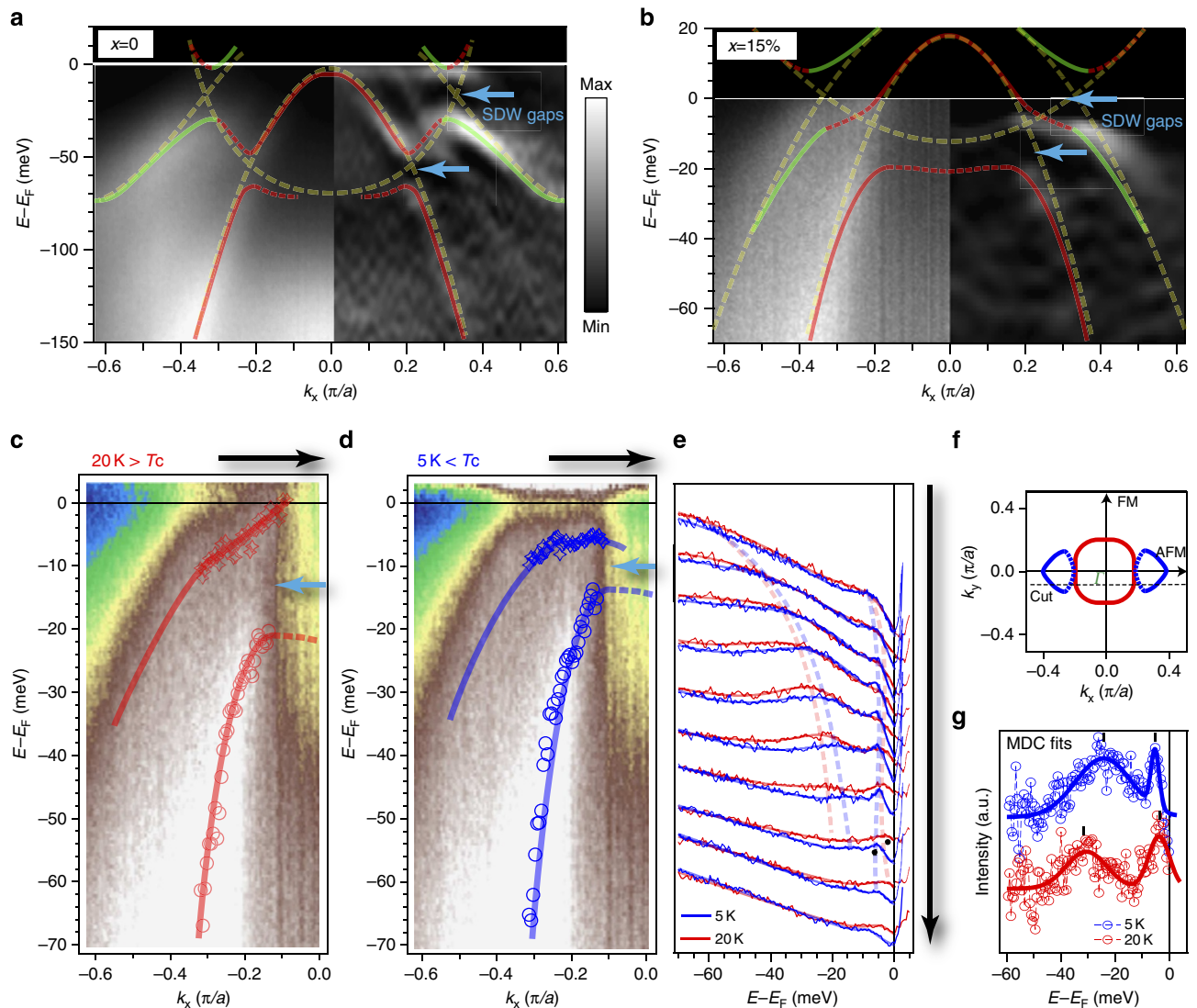


Figure 2 | Suppression of SDW gap below T_c . (a) Band dispersions of BaFe₂As₂ measured in the SDW state (10 K) near Γ as labelled in (f). The left-hand side is the raw image, the right-hand side the second energy derivative. Guides to the eye for the dispersions are marked in colour, highlighting the dominant orbital character (red for d_{xz} ; green for d_{yz}). As the dispersions are the result of SDW folding and gapping, the inferred bands before SDW gapping are marked by yellow dashed lines. (b) Same as a but for the UD ($x=0.15$) sample, measured in the SDW state above T_c at 20 K. (c) The band dispersions from b near the SDW gap taken above T_c , divided by the Fermi-Dirac function convolved with a Gaussian representing instrument resolution. Open symbols are fitted peak positions of the energy distribution curves (EDCs) indicating the band dispersions. Blue arrow points to the SDW gap in discussion. (d) Same measurement but taken below T_c , at 5 K. (e) Comparison of EDCs taken above T_c (red, 20 K) and below T_c (blue, 5 K) across the SDW gap in the momentum range marked by the black arrows in (c,d). Dashed lines trace out the band dispersions. Black circles highlight opening of the SC gap at k_F . (f) Schematic of the reconstructed FS in the SDW state. (g) The momentum distribution curves of (c,d) are fitted with two Lorentzians and a linear background. The intensity of the inner hole band is plotted above (red) and below (blue) T_c , where the separation of the two prominent peaks (black marks), measuring the effective SDW gap, shrinks below T_c . Measurements were taken with 25 eV photons.

gap size reflects the order parameter. The modelling presented here serves to demonstrate the effects of the competition on the electronic spectra.

Detailed temperature dependence. Finally, we can trace the temperature-dependent evolution of this SDW gap by tracking the EDCs across the SDW gap (Fig. 4a), where the separation between the two peaks at each temperature represents the effective SDW gap magnitude. The SDW gap forms below T_{SDW} , but instead of monotonically increasing with decreasing temperature as in BaFe₂As₂, it dips at the onset of SC (Fig. 4c). This behaviour is reminiscent of that of the orthorhombicity and

magnetic moment observed in UD compounds^{20,21}. To complete this comparison, we also plot the temperature dependence of the SC gap on the same inner hole band, which onsets at T_c (Fig. 4b,c). Here, we note that the observed reduction in the SDW gap ($\sim 30\%$) seems much larger than that in the moment ($\sim 4\%$) for this doping^{20,21}. The reason is that this observed decrease in the gap is actually a combined result of three effects: (i) opening of the SC gap pushing down the upper branch; (ii) reduction of Δ_{SDW} ; and (iii) reduction of Δ_S , which occur constructively at this particular momentum to magnify the effect. Depending on the precise interplay of these three ingredients, the overall effect at other momenta could be smaller, but the observed reduction in SDW gap is not limited to this momentum

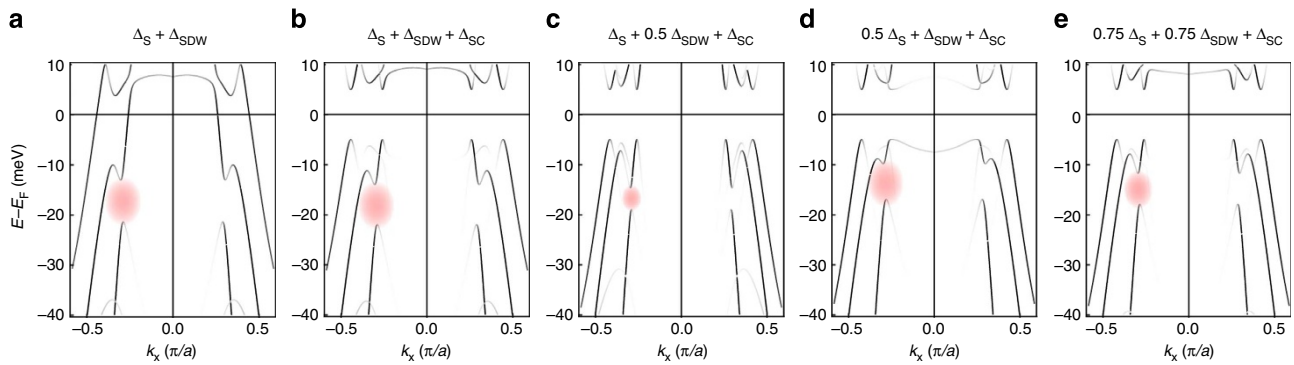


Figure 3 | Model simulation for the three order parameters. A tight-binding fit of BaFe₂As₂ to DFT band structure is used, with a shift of 0.15 eV of the chemical potential and a renormalization factor of 3 to match the measured dispersion of the UD compound. The three order parameters are introduced phenomenologically to understand the effect on spectroscopy: (Δ_S , Δ_{SDW} , Δ_{SC} , associated with T_S , T_{SDW} , T_C). Calculations for the same cut as that in Fig. 2 are plotted here, with the SDW gap highlighted in pink. **(a)** Bands with only finite Δ_S and Δ_{SDW} , mimicking the situation in the orthorhombic SDW state above T_C . **(b)** Simple addition of finite Δ_{SC} with no change in Δ_S and Δ_{SDW} , opening a SC gap at E_F . The SDW gap is not much affected. **(c)** With addition of finite Δ_{SC} and a reduced Δ_{SDW} , the SDW gap size is reduced, but the centre does not shift. **(d)** With the addition of finite Δ_{SC} and reduced Δ_S , the effective SDW gap size is not much affected, but the gap centre shifts up. **(e)** When Δ_S and Δ_{SDW} are both moderately reduced, the effective SDW gap is both reduced in size and shifted up in energy, best matching the experimental observations.

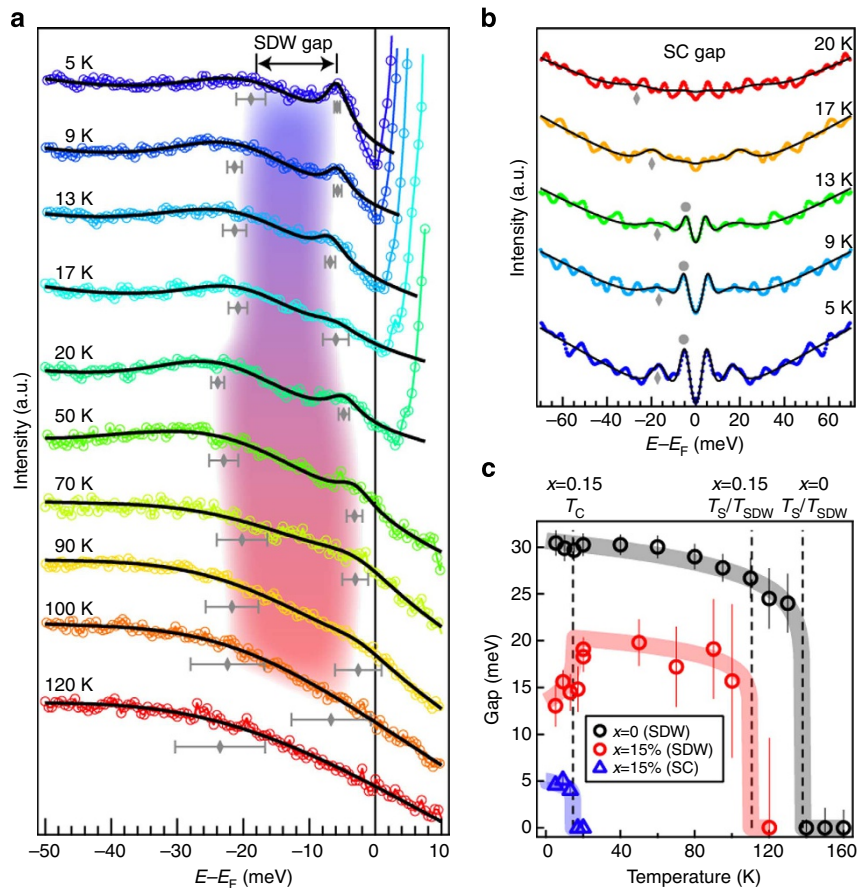


Figure 4 | Temperature dependence of the SDW and SC gaps. **(a)** EDCs divided by Fermi-Dirac function convolved with a Gaussian representing instrumental resolution taken across the SDW gap (integrated EDCs within a $\Delta k_x = 0.05\pi/a$ momentum range centred on the SDW gap for each temperature) as in Fig. 2c from above T_S/T_{SDW} to below T_C . Each EDC is fitted with two Lorentzians and a linear background, with the fit shown by the black curve. Diamonds indicate the peak positions above and below the SDW gap, where the error bars indicate the standard deviations from the fits. Shaded region indicates the effective SDW gap as a function of temperature. **(b)** Symmetrized EDCs at the k_F point of the band crossing as in Fig. 2c, for temperatures across T_C . Diamonds indicate lower branch of the SDW gap, circles indicate superconducting peaks. Black lines are symmetrized fits to the symmetrized EDCs with the Norman model³⁴ for the SC gap, a Lorentzian for the SDW peak, and a second order polynomial for the background. **(c)** The extracted effective SDW gap size for the undoped (black) and UD compound (red), along with the extracted SC gap size for the UD compound (blue), as a function of temperature. The error bars are from the properly combined s.d. of the fitted positions of the two peaks in each EDC marking the upper and lower edges of the SDW gaps.

(Supplementary Note 3). To further confirm such behaviour, we have performed mean-field calculations using tight-binding fits to the DFT-derived bands, including an ad-hoc isotropic SC order parameter and self-consistently determined orbital-dependent SDW. The results show that the introduction of SC indeed suppresses the SDW gaps, as naively expected from the usual interplay between SC and magnetism, where SC gaps quasiparticles around the Fermi surface, leaving much less spectral weight to simultaneously form the SDW order. The temperature dependence of the Δ_{SDW} follows a trend similar to that shown in Fig. 4c; (Supplementary Note 4).

Discussion

The coexistence of magnetism and SC holds a special fascination in the field of HTSC as magnetism is generally believed to be detrimental to SC^{29,30}. Extensive efforts have been made to understand whether this coexistence in the pnictides is indeed microscopic as it would have strong implications on the mechanism of SC in these compounds. In particular, theoretical work has shown that a conventional s_{++} pairing symmetry state cannot coexist with the SDW order, whereas such coexistence is possible for an unconventional s_{\pm} pairing symmetry³¹. Using a simple simulation of the APRES spectra, we show that our observation of the reduced SDW gap and its shift towards E_F as well as the observation of a well-defined superconducting gap below T_C on the same spectrum cannot be explained by a phase-separated coexistence of these orders but more consistent with a microscopic coexistence scenario (Supplementary Note 5), in agreement with NMR measurements³², pointing to s_{\pm} pairing symmetry for this part of the phase diagram. Furthermore, it is clear from our results that the SDW and nematic orders are not mere spectators to the presence of SC. The SDW gap—a representation of the strength of the coherent electronic excitations of the SDW order—is suppressed with the onset of SC, indicating that the SDW order competes with SC for the same electrons. The fact that a reduction in both Δ_{SDW} and Δ_S is required to fully account for the experimental observations also demonstrates that the SDW order and the electronic nematicity are intimately connected and both are likely in competition with SC in the coexistence region.

Lastly, it is interesting to point out the connection to the cuprates. Traditionally, there have been two main interpretations of the PG phase: (i) a precursor state of SC, (ii) a competing phase to SC. While several recent reports favour the scenario of competition^{1–4}, the elusive nature of the PG complicates the interpretations. Here, we demonstrate clearly with spectroscopic evidence the competition between SC and a well-characterized long-range density wave, which is intriguingly similar to a recent study in cuprates showing a similar suppression of the PG spectral features associated with the onset of SC (M. Hashimoto *et al.* submitted). While the competition in iron pnictides may be simpler than that in the cuprates, the comparison of the two families may provide helpful insights on the mysterious PG phase in the cuprates, and help link the two families for an eventual understanding of the mechanism of unconventional SC.

Methods

Experimental conditions. High-quality single crystals of $\text{Ba}_{1-x}\text{K}_x\text{Fe}_2\text{As}_2$ were grown using the self-flux method¹⁸. Mechanical detwinning of the crystals was performed using a previously reported method⁹. ARPES measurements were carried out at both beamline 5-4 of the Stanford Synchrotron Radiation Lightsources and beamline 10.0.1 of the Advanced Light Source using SCIENTA R4000 electron analysers. The total energy resolution was set to 5 meV and the angular resolution was 0.3°. Single crystals were cleaved *in situ* below 10 K for each measurement. All measurements were done in ultra high vacuum with a base pressure lower than 4×10^{-11} torr.

Tight-binding model simulations. The simulations used in Fig. 3 were produced based on a five-orbital tight-binding model of BaFe_2As_2 from DFT band structure²⁴. The E_F was first shifted down by 0.15 eV to account for the hole doping. The bands were then renormalized by a factor of 3 to match the observed band structure for the UD compound. The cut of the calculations shown in Fig. 3 was along $k_y = 0.07\pi/a$, to match the experimental cut shown in Fig. 2. The parameters used in Fig. 3 were implemented as described in the following. The orbital anisotropy, Δ_S , is an onsite energy splitting between d_{xz} and d_{yz} that is momentum dependent ($\Delta_S(\mathbf{k}) = \alpha \cdot \sin^2((|k_x| + |k_y|)/2)$, which is zero at Γ and maximum at X/Y along the high-symmetry directions, and also periodic in k , see Supplementary Note 1), where $\alpha\{d_{xz}, d_{yz}\} = \{-20 \text{ meV}, 40 \text{ meV}\}$. The SDW order parameter, Δ_{SDW} , is diagonal in the orbital basis, with $\Delta_{\text{SDW}}\{d_{xz}, d_{yz}, d_{x^2-y^2}, d_{xy}, d_{3z^2-r^2}\} = 30 \text{ meV} \cdot \{0.25, 1, 0.25, 0.5, 0.25\}$. The ratios between the different orbitals are consistent with the results of self-consistent calculations for the SDW order in the orbital basis, in which d_{yz} bands tend to open the largest SDW gap³³. The superconducting order parameter, Δ_{SC} , is taken to be isotropic and 5 meV.

References

- Kondo, T. *et al.* Competition between the pseudogap and superconductivity in the high- T_C copper oxides. *Nature* **457**, 296–300 (2009).
- Vishik, I. *et al.* Phase competition in trisected superconducting dome. *PNAS* **109**, 18332–18337 (2012).
- Ghiringhelli, G. *et al.* Long-range incommensurate charge fluctuations in $(\text{Y,Nd})\text{Ba}_2\text{Cu}_3\text{O}_{6+x}$. *Science* **337**, 821–825 (2012).
- Chang, J. *et al.* Direct observation of competition between superconductivity and charge density wave order in $\text{YBa}_2\text{Cu}_3\text{O}_{6.67}$. *Nat. Phys.* **8**, 871–876 (2012).
- de la Cruz, C. *et al.* Magnetic order versus superconductivity in the iron-based layered $\text{La}(\text{O}_{1-x}\text{F}_x)\text{FeAs}$ systems. *Nature* **453**, 899–902 (2008).
- Huang, Q. *et al.* Neutron-diffraction measurements of magnetic order and a structural transition in the parent BaFe_2As_2 compound of FeAs-based high-temperature superconductors. *Phys. Rev. Lett.* **101**, 257003 (2008).
- Chu, J.-H. *et al.* In-plane resistivity anisotropy in an underdoped iron arsenide superconductor. *Science* **329**, 824–826 (2010).
- Tanatar, M. A. *et al.* Uniaxial-strain mechanical detwinning of CaFe_2As_2 and BaFe_2As_2 crystals: optical and transport study. *Phys. Rev. B* **81**, 184508 (2010).
- Yi, M. *et al.* Symmetry-breaking orbital anisotropy observed for detwinned $\text{Ba}(\text{Fe}_{1-x}\text{Co}_x)_2\text{As}_2$ above the spin density wave transition. *PNAS* **108**, 6878–6883 (2011).
- Kasahara, S. *et al.* Electronic nematicity above the structural and superconducting transition in $\text{BaFe}_2(\text{As}_{1-x}\text{P}_x)_2$. *Nature* **486**, 382–385 (2012).
- Wang, A. F. *et al.* A crossover in the phase diagram of $\text{NaFe}_{1-x}\text{Co}_x\text{As}$ determined by electronic transport measurements. *New J. Phys.* **15**, 043048 (2013).
- Stewart, G. R. Superconductivity in iron compounds. *Rev. Mod. Phys.* **83**, 1589–1652 (2011).
- Rotter, M., Tegel, M. & Johrendt, D. Superconductivity at 38 K in the iron arsenide $(\text{Ba}_{1-x}\text{K}_x)\text{Fe}_2\text{As}_2$. *Phys. Rev. Lett.* **101**, 107006 (2008).
- Zhao, J. *et al.* Structural and magnetic phase diagram of $\text{CeFeAsO}_{1-x}\text{F}_x$ and its relation to high-temperature superconductivity. *Nat. Mat.* **7**, 953–959 (2008).
- Parker, D. R. *et al.* Control of the competition between a magnetic phase and a superconducting phase in cobalt-doped and nickel-doped NaFeAs using electron count. *Phys. Rev. Lett.* **104**, 057007 (2010).
- Chu, J.-H. *et al.* Determination of the phase diagram of the electron-doped superconductor $\text{Ba}(\text{Fe}_{1-x}\text{Co}_x)_2\text{As}_2$. *Phys. Rev. B* **79**, 014506 (2009).
- Ni, N. *et al.* Effects of Co substitution on thermodynamic and transport properties and anisotropic H_{c2} in $\text{Ba}(\text{Fe}_{1-x}\text{Co}_x)_2\text{As}_2$ single crystals. *Phys. Rev. B* **78**, 214515 (2008).
- Shen, B. *et al.* Transport properties and asymmetric scattering in $\text{Ba}_{1-x}\text{K}_x\text{Fe}_2\text{As}_2$ single crystals. *Phys. Rev. B* **84**, 184512 (2011).
- Nandi, S. *et al.* Anomalous suppression of the orthorhombic lattice distortion in superconducting $\text{Ba}(\text{Fe}_{1-x}\text{Co}_x)_2\text{As}_2$ single crystals. *Phys. Rev. Lett.* **104**, 057006 (2010).
- Avci, S. *et al.* Magnetoelastic coupling in the phase diagram of $\text{Ba}_{1-x}\text{K}_x\text{Fe}_2\text{As}_2$ as seen via neutron diffraction. *Phys. Rev. B* **83**, 172503 (2011).
- Wiesenmayer, E. *et al.* Microscopic coexistence of superconductivity and magnetism in $\text{Ba}_{1-x}\text{K}_x\text{Fe}_2\text{As}_2$. *Phys. Rev. Lett.* **107**, 237001 (2011).
- Yi, M. *et al.* Electronic reconstruction through the structural and magnetic transitions in detwinned NaFeAs . *New J. Phys.* **14**, 073019 (2012).
- Kuo, H.-H. *et al.* Magnetoelastically coupled structural, magnetic, and superconducting order parameters in $\text{BaFe}_2(\text{As}_{1-x}\text{P}_x)_2$. *Phys. Rev. B* **86**, 134507 (2012).
- Graser, S. *et al.* Spin fluctuations and superconductivity in a three-dimensional tight-binding model for BaFe_2As_2 . *Phys. Rev. B* **81**, 214503 (2010).
- Kruger, F., Kumar, S., Zaanen, J. & van den Brink, J. Spin-orbital frustrations and anomalous metallic state in iron-pnictide superconductors. *Phys. Rev. B* **79**, 054504 (2009).
- Chen, C.-C. *et al.* Finite-temperature spin dynamics and phase transitions in spin-orbital models. *Phys. Rev. B* **80**, 180418 (2009).

27. Daghofer, M. *et al.* Orbital-weight redistribution triggered by spin order in the pnictides. *Phys. Rev. B* **81**, 180514 (2010).
28. Dai, P., Hu, J. & Dagotto, E. Magnetism and its microscopic origin in iron-based high-temperature superconductors. *Nat. Phys.* **8**, 709–718 (2012).
29. Berk, N. F. & Schrieffer, J. R. Effect of ferromagnetic spin correlations on superconductivity. *Phys. Rev. Lett.* **17**, 433–435 (1966).
30. Schieffer, J. R., Wen, X. G. & Zhang, S. C. Dynamic spin fluctuations and the bag mechanism of high- T_C superconductivity. *Phys. Rev. B* **39**, 11663–11679 (1989).
31. Fernandes, R. & Schmalian, J. Competing order and nature of the pairing state in the iron pnictides. *Phys. Rev. B* **82**, 014521 (2010).
32. Li, Z. *et al.* Microscopic coexistence of antiferromagnetic order and superconductivity in $\text{Ba}_{0.77}\text{K}_{0.23}\text{Fe}_2\text{As}_2$. *Phys. Rev. B* **86**, 180501(R) (2012).
33. Plonka, N., Kemper, A. F., Graser, S., Kampf, A. P. & Devereaux, T. P. Tunneling spectroscopy for probing orbital anisotropy in iron pnictides. *Phys. Rev. B* **88**, 174518 (2013).
34. Norman, M. R., Randeria, M., Ding, H. & Campuzano, J. C. Phenomenology of the low-energy spectral function in high- T_C superconductors. *Phys. Rev. B* **57**, R11093–R11096 (1998).

Acknowledgements

ARPES experiments were performed at the Stanford Synchrotron Radiation Lightsource and the Advanced Light Source, which are both operated by the Office of Basic Energy Sciences, U.S. Department of Energy. The Stanford work is supported by the US DOE,

Office of Basic Energy Science, Division of Materials Science and Engineering, under Award # DE-AC02-76SF00515.

Author contributions

M.Y. and D.H.L. conceived the project. M.Y., Y.Z. and Z.-K.L. took the measurements. M.Y. analysed the data. X.D. grew the UD single crystals. J.-H.C. grew the undoped single crystals. A.F.K., N.P. and B.M. performed the calculations and provided theoretical insights. M.H. and S.-K.M. assisted in ARPES measurements at SSRL and ALS. Z.H., T.P.D., I.R.F. and H.H.W. provided guidance. Z.-X.S. and D.H.L. oversaw the project. M.Y. and D.H.L. wrote the paper with input from all coauthors.

Additional information

Supplementary Information accompanies this paper at <http://www.nature.com/naturecommunications>

Competing financial interests: The authors declare no competing financial interests.

Reprints and permission information is available online at <http://npg.nature.com/reprintsandpermissions/>

How to cite this article: Yi, M. *et al.* Dynamic competition between spin-density wave order and superconductivity in underdoped $\text{Ba}_{1-x}\text{K}_x\text{Fe}_2\text{As}_2$. *Nat. Commun.* 5:3711 doi: 10.1038/ncomms4711 (2014).